

Pathfinders of the Pacific Ocean Neutrino Experiment

Kilian Holzapfel,^a Braeden Veenstra,^b Li Ruohan,^a Patrick Hatch^c and Christian Spannfellner^{a,*} for the P-ONE collaboration

^a*Technische Universität München,
James-Franck-Straße, 85748, Garching, Germany*

^b*University of Alberta,
4-181 CCIS Edmonton, Alberta, Canada T6G 2E1*

^c*Queen's University,
64 Bader Ln, Kingston, Ontario, Canada K7L 3N6*

E-mail: kilian.holzapfel@tum.de, btveenst@ualberta.ca

The Pacific Ocean Neutrino Experiment (P-ONE) is a proposed neutrino telescope located off the coast of Vancouver Island, Canada. With a planned instrumented volume of over one cubic kilometer, P-ONE aims to measure high-energy neutrinos to gain further insights into astrophysical accelerators and the cosmos. However, the dynamic ocean environment presents challenges, such as changing ocean currents influencing the detector geometry and the bioluminescent light background. The P-ONE collaboration, in association with Ocean Networks Canada (ONC), is developing durable deep-sea detector systems to overcome these challenges. In 2018 and 2020, respectively, the pathfinder experiments STRAW (STRings for Absorption length in Water) and STRAW-b were deployed to characterize and monitor the optical properties and the background light caused by bioluminescence and K40 in the Cascadia Basin. These pathfinders include three strings with diverse instruments such as spectrometers, LiDARs, cameras, and early prototype optical modules. An overview of recent findings from the STRAW and STRAW-b measurements will be presented.

38th International Cosmic Ray Conference (ICRC2023)
26 July - 3 August, 2023
Nagoya, Japan



*Speaker

1. Pacific Ocean Neutrino Experiment and its Pathfinder Missions

The Pacific Ocean Neutrino Experiment (P-ONE) is a joint initiative among universities and research institutions in the USA, Canada, UK, Poland, and Germany to construct a multi-cubic-kilometer neutrino telescope in the Pacific Ocean that will provide new insights into the Universe's highest energies [1, 2]. The project began in 2017 and has since developed into an international collaboration. The primary partner of P-ONE is Ocean Networks Canada (ONC), an initiative from the University of Victoria that operates NEPTUNE, which is the most extensive oceanographic infrastructure globally [3]. The NEPTUNE ocean observatory provides power and data connections to various deep ocean sites off the west coast of Vancouver Island as depicted in Figure 1. For P-ONE, the Cascadia Basin with a depth of 2660 m has been selected due to its expanded flat seafloor. This site has been under observation since 2018 by two pathfinder experiments, namely Strings for Absorption Length in Water (STRAW) (Section 1.1) and STRAW-b (Section 1.2), to qualify the environmental properties. Following up on the two pathfinder experiences, the design of P-ONE started, and the blueprint of the P-ONE mooring line is currently under design, with a deployment scheduled in 2024 [2].

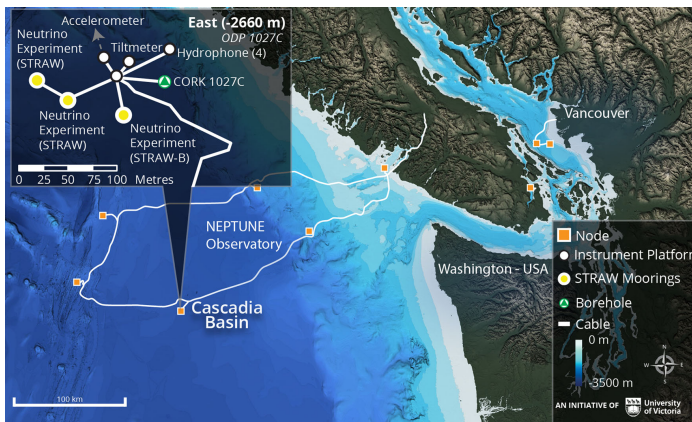


Figure 1: Map of ONC's NEPTUNE Observatory. P-ONE will be located at the Cascadia Basin node, where the pathfinder projects STRAW and STRAW-b are operating. Image courtesy of ONC.

1.1 First Pathfinder: Strings for Absorption Length in Water (STRAW)

The Strings for Absorption Length in Water (STRAW) is the first pathfinder mission towards P-ONE. As the name indicates, STRAW's primary purpose is to assess the attenuation length of water in the wavelength range of 350 nm to 600 nm and the optical background at the site where the P-ONE will be constructed. Besides, gaining experience in the challenges of deep-sea experiments is another purpose of the STRAW mission [4, 5].

STRAW has two 146 m long mooring lines with 37-m horizontal spacing. Each mooring hosts four modules. From the overall eight modules, three modules are called Precision Optical Calibration Module (POCAM) and emit calibrated, intense, adjustable, isotropic, nanosecond light flashes [4]. The remaining five modules are called STRAW Digital Optical Module (sDOM) and detect the light with one up- and one down-facing 3-inch photomultiplier tube (PMT)[4]. The modules are placed along the mooring line above the sea floor at a depth of 30 m to 110 m. STRAW's geometry allows to record the light intensity of each POCAM at different distances with the sDOM, which translates to a relative intensity measurement instead of a more complex absolute measurement [4, 5].

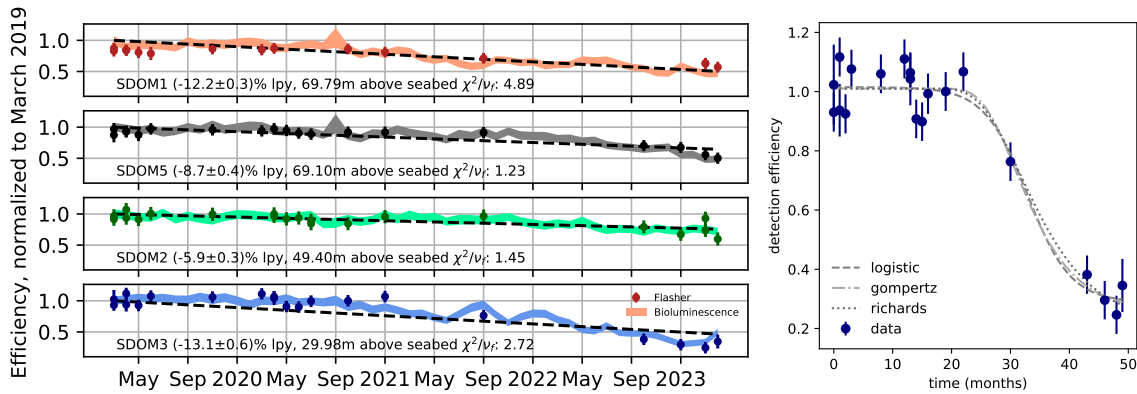


Figure 2: Evolution of STRAW optical modules with four years of data (left) and normalized fraction of detected pulses from the flasher for the deepest sDOM (right). Best fit curves are shown for three biologically motivated models. Included are the Unified Richards model [6], logistic [6, 7] and non re-parameterised Gompertz [8] models, which have all been employed in broad contexts, including the growth of microorganisms [6, 7, 9].

1.2 Second Pathfinder: Strings for Absorption Length in Water b (STRAW-b)

STRAW-b is the second pathfinder for P-ONE deployed in 2020, positioned approximately 40 m away from STRAW. The motivation for STRAW-b is to gain experience deploying a longer mooring line and further characterizing environmental parameters such as bioluminescence. It consists of ten modules mounted on a 444-meter-long mooring line. With one exception, all modules are equipped with a 13-inch high-pressure-resistant glass housing for added protection. To ensure redundancy, each module is connected to its data cable, which provides network connection via glass fibers and power supply with copper cables and is connected to the junction box at the base of the line. Each module incorporates environmental sensors, including internal pressure, temperature, and humidity which serve as checkpoints for the successful deployment and long-term monitoring of the module’s health. In addition, an accelerometer and electronic compass measure the module’s orientation, shielding information of the mooring movements with the currents [4]. Among those modules, there are two modules which are characterizing the bioluminescence emissions with a low-light camera. The modules are placed at a depth of 2252 m and 2516 m from the surface which translates to 408 m and 144 m from the seafloor, respectively [4].

2. Biofouling

Figure 2 shows the preliminary result of sDOM efficiency evolution due to biofouling and sedimentation. The depth of each optical module is shown. Two independent measurements were used to extract the efficiency loss. The first measurement is shown as a thick band, with the width of the band indicating a $\pm 1\sigma$ confidence interval. It used the ambient light due to bioluminescence, which comes from STRAW’s continuous data taking mode [5]. For each month since March 2019, the average light seen by both upwards and downwards facing PMTs was calculated. A time interval of one month was used for averaging any large fluctuations due to tidal effects. Since fouling accumulates faster on up-facing substrates, the ratio of the up- and down-facing light was chosen as an estimator for the efficiency change over time [10]. The second measurement is shown as points,

which were measured using the POCAM flashers pulsed with a known frequency. The fraction of detected flashes were measured. A linear least-squares fit was used to fit a scaling factor which provides the best match between the two data sets. Uncertainties from the fitting process were propagated onto individual data points in order to account for systematic effects. The reduced χ^2 between the two modules is also shown for each optical module. A linear fit was performed and the results are shown by the dashed lines in Figure 2. The slope of each fit is indicated as a percentage loss per year. All up-facing optical surfaces show a loss in transparency based on this analysis.

A potential driver for the changes observed in the STRAW modules is the growth of colonies of microorganisms. The literature describing models for population growth is extensive [7, 9]. Figure 2 shows a selection of candidate models to describe the observed evolution of the optical modules. Further analysis could provide insight into the development of these microorganism colonies. The transition delay, light absorption once the maximum population is reached, and the dynamics of this transition phase are the key parameters of interest for physics with neutrino telescopes.

3. Bioluminescence

Bioluminescence is a deep-sea phenomenon, which refers to the emission of light by living organisms such as bacteria, plankton, and fish. While bioluminescence is a crucial aspect of oceanography, it poses a significant background for neutrino telescopes. Therefore P-ONE requires a deep understanding of the physical and biological processes that contribute to bioluminescence, as well as the use of advanced modeling techniques to simulate and account for its effects. Despite this challenge, bioluminescence in neutrino telescopes offers a unique opportunity for biologists to study life in the deep-sea, which is by far the most extensive habitat on Earth and still remains largely unexplored.

Since mid-2021, the cameras installed in STRAW-b have consistently captured images. Due to limited bandwidth for camera communication, the image capture process involves a 63.5 s exposure followed by a 36 s period for image download. This sequence, totaling 99.5 s, has been repeating with an

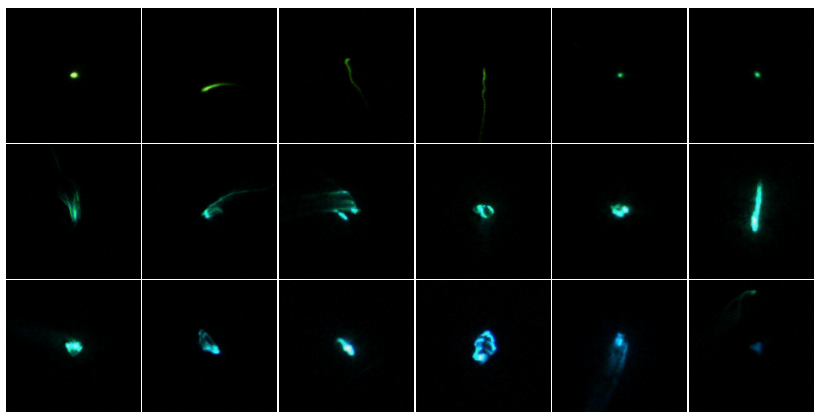


Figure 3: Hues of the deep-sea. A selection of bioluminescence emissions, sorted by their hue (top left to bottom right). All images have the same zoom level. Remarkable is the last image with two different emission colors.

uptime exceeding 95 % since May 2021, resulting in a collection of over 1 million recorded images. It is important to note that most of these images do not depict any instances of bioluminescence. To address this, an innovative image recognition algorithm, supported by machine learning (ML), was developed and trained to identify and extract bioluminescent emissions. A selection of detected bioluminescence is depicted in Figure 3. Additionally, the algorithm extracts pertinent information for each detected emission, such as intensity and position within the image. These characteristics

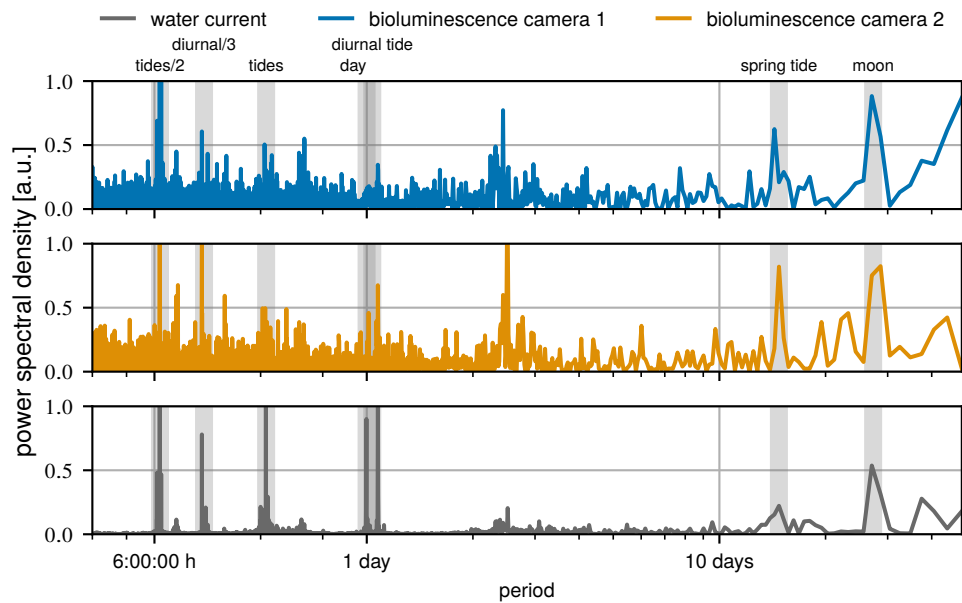


Figure 4: Periodogram of the water currents and the bioluminescence appearance in images. Important periods are marked. The x-axis is in logarithmic scale to cover the total range of periods and labeled with time classical nomenclature for readability.

of the detected bioluminescent emissions are the foundation for various analyses in the subsequent subsections.

3.1 Periodicity in Bioluminescence Rates

The detection of bioluminescence events by the cameras at the future site of P-ONE exhibits temporal variability. This behavior can be attributed to two factors. Firstly, bioluminescence occurs when organisms experience external forces, either through collisions with objects or due to shear forces arising from water turbulence [11–13]. Secondly, water currents exhibit temporal variations. An advantage of the Cascadia Basin site is that ONC has deployed multiple devices to measure current speeds for over a decade. A periodic analysis of the current speeds and bioluminescence rates reveals similar dominant periods, which can be correlated with tidal periods, as depicted in Figure 4.

4. Spectral Population of Bioluminescent Organisms

Bioluminescence emission is biased towards blue light due to its better propagation in water. However, the emission spectra can vary depending on the emitting species and the underlying biochemical reaction. For many organisms, the emission spectra are known and can be expressed as a spectral catalog of bioluminescence [11]. Since the camera captures images in three different color channels (RGB), obtaining spectral information of an emission requires a special treatment outlined in the following. First, the RGB color gets transformed to a color angle known as hue. The resulting hue distribution of all detected emissions can be simulated by incorporating the transmittance spectra of the water and the glass housing, the spectral response of the camera, and a spectral population of bioluminescent organisms.

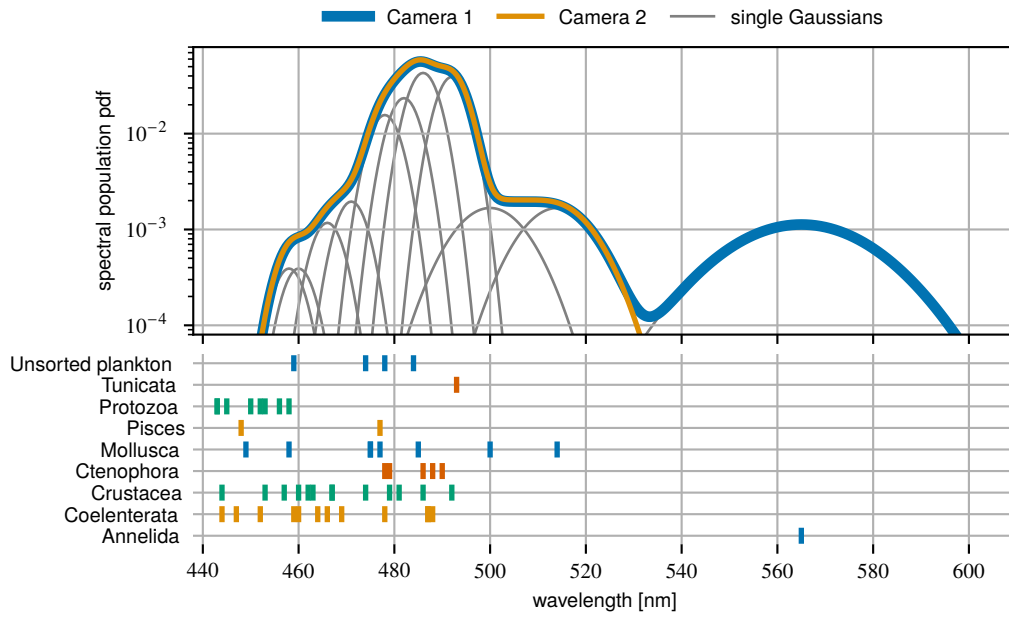


Figure 5: Spectral bioluminescence population to reproduce the hues distribution measured with the cameras. The distribution describes the population of Gaussian emitters, each with a FWHM of 82 nm. The lower plot shows the peak positions of listed organisms in the bioluminescence catalog [11].

Figure 5 illustrates the resulting spectral population to reproduce the detected hue distribution. Furthermore, it includes a representation of the bioluminescence catalog [11, 14]. The detected spectral populations align with the bioluminescence catalog because the primary peak position is located around 485 nm, where the catalog reports the emission spectra of many animals. Remarkable is the population around 565 nm, which only appears in Camera 1 (located closer to the ground). Assuming that the bioluminescence catalog covers all the species present in the Cascadia Basin, the peak at 565 nm can be attributed to *Tomopteris nisseni*. This species belongs to the segmented worm group (*Annelida*) and is reported to be planktonic, indicating that it cannot move against water currents [11, 14].

4.1 Bioluminescence Emission Rate, Water Flow and Concentration of Emitting Organisms

As mentioned before, there are essentially two reasons why organisms produce bioluminescence: one is due to contact forces when they come into contact with an object, and the other is a result of shear forces caused by turbulent surroundings. Spontaneous emissions can be neglected due to the rare probability because each emission is an energy investment for the organisms, and energy is rare in the deep-sea [11–13]. Therefore the bioluminescence emission rate induced around an object is $R = R_{\text{contact}} + R_{\text{shear}}$. The contact emission rate can be expressed by $R_{\text{contact}} = c_{\text{bio}} A_{\perp} p_{\text{contact}} |\vec{v}|$ with the flow velocity \vec{v} , the cross sectional area of the object A_{\perp} and the concentration of bioluminescent organisms c_{bio} in the water. The cross sectional area A_{\perp} is the area that is normal to the direction of flow \vec{v} . p_{contact} denotes the emission probability and is approximately constant [15]. The emission probability due to shear stress is linearly connected to the water current's gradient with $p_{\text{shear}}(\vec{u}) \sim \alpha \nabla \vec{u}$ where α is a proportionality factor [16–18]. The rate from shear stress can be expressed by the divergence theorem and an effective cross sectional area $A_{\perp}^*(\vec{u})$ covering the entire

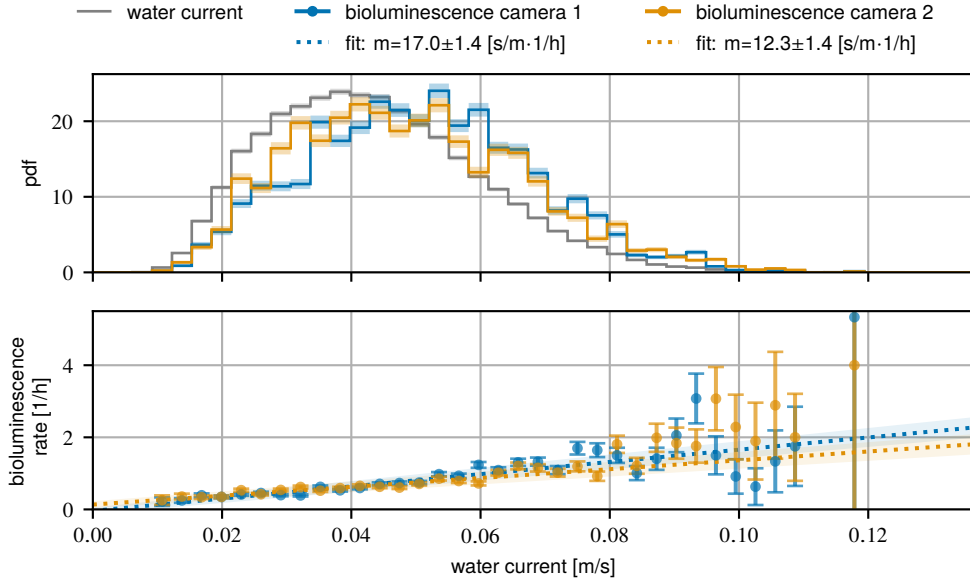


Figure 6: The upper plot displays the probability density functions (PDFs) of the measured flow speeds $f_V(|\vec{u}|)$ (shown in gray) and the flow speeds during which bioluminescence occurrences took place $f_{V \cap B}(|\vec{u}|)$. The lower plot demonstrates the expected linear dependence between the emission rate and flow speed, which is derived in the text.

flow disturbance downstream of an object. For the expected flow speeds 5 cm s^{-1} to 20 cm s^{-1} , the flow around the detector objects is in the regime where vortex streets appear downstream of the objects. There A_{\perp}^* can be assumed constant because the vortex streets have a fixed size which is a constraint of the stability of the vortex street. Indeed the vortex street osculation can be measured by the magnetic compass sensor of STRAW-b modules with an amplitude up to 5° . Hence, the rate of bioluminescence emissions is proportional to the flow speed with

$$R(|\vec{u}|) = c_{\text{bio}} (A_{\perp} p_{\text{contact}} + \alpha A_{\perp}^*) |\vec{u}|. \quad (1)$$

To show this relationship in the data, it is necessary to establish a connection between the measured current speeds and the detected bioluminescence in the captured images. To make the analysis statistically robust against the low bioluminescence emission rate, $R(|\vec{u}|)$ can be expressed by

$$R(|\vec{u}|) = \frac{N}{T} \frac{f_{V \cap B}(|\vec{u}|)}{f_V(|\vec{u}|)} \quad (2)$$

with the PDFs of the current speed f_V and the current speed $f_{V \cap B}$ during which the condition B of an emission occurrence holds. Furthermore, T is the total duration of the data, and N is the total number of emissions. The current speeds at Cascadia Basin are recorded using a currentmeter positioned 2.1 km northwest of STRAW-b. Finally, both cameras yield a similar concentration of $0.03(3) \text{ m}^{-3}$ of emitting organisms, including the systematic error, which agrees with the range of 0.622 m^{-3} to 0.018 m^{-3} measured in ANTARES [19].

5. Conclusion

The pathfinder missions have yielded crucial information about the suitability of Cascadia Basin for the potential construction of a large-scale neutrino telescope P-ONE. Additionally, the successful implementation of the STRAW and STRAW-b projects has demonstrated the effectiveness of collaborating with the ONC in terms of ensuring reliable deep-sea deployments and operations. Furthermore, these pathfinder missions have also gathered data on various aspects, such as the water's attenuation length, the growth of bio-fouling, and the characterization of the light background for detecting neutrinos emitted by ^{40}K and bioluminescence [5].

References

- [1] M. Agostini et al., *Nature Astronomy* **2020**, *4*, 913–915.
- [2] E. Resconi, Towards a new neutrino telescope in the Pacific Ocean, **2023**.
- [3] C. R. Barnes et al., *IEEE Journal of Oceanic Engineering* **2013**, *38*, 144–157.
- [4] M. Boehmer et al., *Journal of Instrumentation* **2019**, *14*, P02013–P02013.
- [5] N. Bailly et al., *The European Physical Journal C* **2021**, *81*.
- [6] E. Tjørve and K. M. C. Tjørve, *Journal of Theoretical Biology* **2010**, *267*, 417–425.
- [7] D. Charlebois and G. Balázsi, *In Silico Biology* **2019**, *13*, 21–39.
- [8] K. M. C. Tjørve and E. Tjørve, *PLOS ONE* **2017**, *12*, e0178691.
- [9] D. López et al., *International Journal of Food Microbiology* **2004**, *96*, 289–300.
- [10] P. Amram et al., *Astropart. Phys.* **2003**, *19*, 253–267.
- [11] M. I. Latz et al., *Marine Biology* **1988**, 441–446.
- [12] A. Gouveneaux, PhD thesis, **2016**.
- [13] P. J. Herring, *Proceedings of the Royal Society of London. Series B. Biological Sciences* **1983**, *220*, 183–217.
- [14] W. Francis et al., *Luminescence* **2014**, *29*.
- [15] J. Rohr et al., **1994**.
- [16] E. M. Maldonado et al., *The Biological Bulletin* **2007**, *212*, 242–249.
- [17] J. Rohr et al., *Journal of Experimental Biology* **1998**, *201*, 1447–1460.
- [18] S. Meighen-Berger et al., Bioluminescence modeling for deep sea experiments, **2021**.
- [19] I. G. Priede et al., *Deep Sea Research Part I: Oceanographic Research Papers* **2008**, *55*, 1474–1483.

Full Authors List: P-ONE Collaboration

Matteo Agostini¹¹, Nicolai Bailly¹, A.J. Baron¹, Jeannette Bedard¹, Chiara Bellenghi², Michael Böhmer², Cassandra Bosma¹, Dirk Brussow¹, Ken Clark³, Beatrice Crudele¹¹, Matthias Danninger⁴, Fabio De Leo¹, Nathan Deis¹, Tyce DeYoung⁶, Martin Dinkel², Jeanne Garriz⁶, Andreas Gärtner⁵, Roman Gernhäuser², Dilraj Ghuman⁴, Vincent Gousy-Leblanc², Darren Grant⁶, Christian Haack¹⁴, Robert Halliday⁶, Patrick Hatch³, Felix Henningsen⁴, Kilian Holzapfel², Reyna Jenkyns¹, Tobias Kerscher², Shane Kerschtiel¹, Konrad Kopański¹⁵, Claudio Kopper¹⁴, Carsten B. Krauss⁵, Ian Kulin¹, Naoko Kurahashi¹², Paul C. W. Lai¹¹, Tim Lavalley¹, Klaus Leismüller², Sally Leys⁸, Ruohan Li², Paweł Malecki¹⁵, Thomas McElroy⁵, Adam Maunder⁵, Jan Michel⁹, Santiago Miro Trejo⁵, Caleb Miller⁴, Nathan Molberg⁵, Roger Moore⁵, Hans Niederhausen⁶, Wojciech Noga¹⁵, Laszlo Papp², Nahee Park³, Meghan Paulson¹, Benoît Pirenne¹, Tom Qiu¹, Elisa Resconi², Niklas Retza², Sergio Rico Agreda¹, Steven Robertson⁵, Albert Ruskey¹, Lisa Schumacher¹⁴, Stephen Sclafani¹², Christian Spannfellner², Jakub Stacho⁴, Ignacio Taboada¹³, Andrii Terliuk², Matt Tradewell¹, Michael Traxler¹⁰, Chun Fai Tung¹³, Jean Pierre Twagirayezu⁶, Braeden Veenstra⁵, Seann Wagner¹, Christopher Weaver⁶, Nathan Whitehorn⁶, Kinwah Wu¹¹, Juan Pablo Yañez⁵, Shiqi Yu⁶, Yingsong Zheng¹

¹Ocean Networks Canada, University of Victoria, Victoria, British Columbia, Canada.

²Department of Physics, School of Natural Sciences, Technical University of Munich, Garching, Germany.

³Department of Physics, Engineering Physics and Astronomy, Queen's University, Kingston, Ontario, Canada.

⁴Department of Physics, Simon Fraser University, Burnaby, British Columbia, Canada.

⁵Department of Physics, University of Alberta, Edmonton, Alberta, Canada.

⁶Department of Physics and Astronomy, Michigan State University, East Lansing, MI, USA.

⁸Department of Biological Sciences, University of Alberta, Edmonton, Alberta, Canada.

¹⁰Gesellschaft für Schwerionenforschung, Darmstadt, Germany.

¹¹ Department of Physics and Astronomy and Mullard Space Science Laboratory, University College London, United Kingdom

¹² Department of Physics, Drexel University, 3141 Chestnut Street, Philadelphia, PA 19104, USA.

¹³ School of Physics and Center for Relativistic Astrophysics, Georgia Institute of Technology, Atlanta, GA, USA.

¹⁴ Erlangen Centre for Astroparticle Physics, Friedrich-Alexander-Universität Erlangen-Nürnberg, D-91058 Erlangen, Germany.

¹⁵ H. Niewodniczański Institute of Nuclear Physics, Polish Academy of Sciences, Radzikowskiego 152, 31-342 Kraków, Poland.

^α now at Department of Physics, University of Maryland, College Park, MD 20742, USA.

Acknowledgments

We thank Ocean Networks Canada for the very successful operation of the NEPTUNE observatory, as well as the support staff from our institutions without whom P-ONE could not be operated efficiently.

We acknowledge the support of Natural Sciences and Engineering Research Council, Canada Foundation for Innovation, Digital Research Alliance, and the Canada First Research Excellence Fund through the Arthur B. McDonald Canadian Astroparticle Physics Research Institute, Canada; European Research Council (ERC), European Union; Deutsche Forschungsgemeinschaft (DFG), Germany; National Science Centre, Poland; U.S. National Science Foundation-Physics Division, USA.

